Impact of Synoptic-Scale Wave Breaking on the NAO and Its Connection with the Stratosphere in ERA-40

TORBEN KUNZ, KLAUS FRAEDRICH, AND FRANK LUNKEIT

Meteorologisches Institut, Universität Hamburg, Hamburg, Germany

(Manuscript received 25 July 2008, in final form 6 April 2009)

ABSTRACT

This observational study investigates the impact of North Atlantic synoptic-scale wave breaking on the North Atlantic Oscillation (NAO) and its connection with the stratosphere in winter, as derived from the 40-yr ECMWF Re-Analysis (ERA-40). Anticyclonic (AB) and cyclonic wave breaking (CB) composites are compiled of the temporal and spatial components of the large-scale circulation using a method for the detection of AB and CB events from daily maps of potential vorticity on an isentropic surface. From this analysis a close link between wave breaking, the NAO, and the stratosphere is found: 1) a positive feedback between the occurrence of AB (CB) events and the positive (negative) phase of the NAO is suggested, whereas wave breaking in general without any reference to AB- or CB-like behavior does not affect the NAO, though it preferably emerges from its positive phase. 2) AB strengthens the North Atlantic eddy-driven jet and acts to separate it from the subtropical jet, while CB weakens the eddy-driven jet and tends to merge both jets. 3) AB (CB) events are associated with a stronger (weaker) lower-stratospheric polar vortex, characterized by the 50-hPa northern annular mode. During persistent weak vortex episodes, significantly more frequent CB than AB events are observed concurrently with a significant negative NAO response up to 55 days after the onset of the stratospheric perturbation. Finally, tropospheric wave breaking is related to nonannular stratospheric variability, suggesting an additional sensitivity of wave breaking and, thus, the NAO to specific distortions of the stratospheric polar vortex, rather than solely its strength.

1. Introduction

The North Atlantic Oscillation (NAO) has been the subject of much research as it represents the dominant mode of low-frequency variability over the North Atlantic and considerably influences European climate and weather (for an overview of the NAO, see, e.g., Hurrell 1995; Hurrell et al. 2003). Although the NAO exhibits substantial interannual and decadal variability, a number of studies have investigated the fundamental role of synoptic-scale processes for its underlying dynamics, from an observational as well as modeling perspective (Feldstein 2000, 2003; Benedict et al. 2004; Franzke et al. 2004; Abatzoglou and Magnusdottir 2006; Rivière and Orlanski 2007; Woollings et al. 2008; Strong and Magnusdottir 2008; Kunz et al. 2009a,b).

In particular, synoptic-scale wave breaking near the tropopause, associated with meridional eddy-momentum fluxes and the generation of large-scale potential vorticity anomalies, has been closely related to the variability of the NAO. Specifically, Benedict et al. (2004), Franzke et al. (2004), and Rivière and Orlanski (2007) suggest that the positive phase of the NAO is driven by anticyclonic wave breaking[1] over North America and the North Atlantic, while cyclonic wave breaking is responsible for the negative phase. This NAO–wave breaking view is further investigated by Kunz et al. (2009b) in a simplified general circulation model, applying a newly developed method for the detection of anticyclonic and cyclonic wave breaking events. Generally, in this picture low-frequency (e.g., monthly or seasonal mean) NAO anomalies may arise simply because of more or less frequent wave breaking events during a given period.

Corresponding author address: Torben Kunz, Meteorologisches Institut, Universität Hamburg, Bundesstraße 55, D-20146 Hamburg, Germany.
E-mail: torben.kunz@zmaw.de

[1] Anticyclonic and cyclonic wave breaking according to the LC1 and LC2 idealized baroclinic wave life cycle, respectively (see, e.g., Thorncroft et al. 1993).

DOI: 10.1175/2009JCLI2750.1

Furthermore, observational and modeling evidence exists for stratospheric impacts on the NAO or tropospheric northern annular mode (NAM), which implies that the stratosphere contributes to their intraseasonal as well as interannual variability (e.g., Baldwin et al. 1994; Baldwin and Dunkerton 2001; Ambaum and Hoskins 2002; Charlton et al. 2004; Scaife et al. 2005). Although the NAO and tropospheric NAM are closely related (Wallace 2000; Ambaum et al. 2001; Vallis et al. 2004; Feldstein and Franzke 2006), it is found that the largest tropospheric response to stratospheric perturbations is associated with the NAO (e.g., Baldwin et al. 1994), and thus we also adopt the NAO framework for the present study.

Different processes have been proposed to explain dynamical stratosphere–troposphere coupling, such as the downward control mechanism by the meridional circulation (Haynes et al. 1991; Thompson et al. 2006), which is equivalent to the geostrophic/hydrostatic adjustment of the troposphere to perturbations of the stratospheric polar vortex, as presented by (Ambaum and Hoskins 2002), and downward planetary wave reflection in the stratosphere (Perlwitz and Harnik 2003). Additionally, the possibility of a downward influence from the lower stratosphere by direct modulation of tropospheric baroclinic waves has been suggested by several studies (Baldwin and Dunkerton 1999, 2001; Baldwin et al. 2003; Kushner and Polvani 2004; Charlton et al. 2004; Wittman et al. 2004; Wittman et al. 2007; Kunz et al. 2009a) in the sense of altered tropospheric synoptic-scale wave breaking characteristics. Thus, North Atlantic synoptic-scale wave breaking should be expected to play a key role for the connection between the stratosphere and the NAO.

Given the amount of evidence for the importance of synoptic-scale wave breaking in the large-scale extratropical circulation, the present study attempts to answer the following question: *What is the impact of North Atlantic synoptic-scale wave breaking on the NAO, and how is it connected to the stratosphere?* For this purpose the wave breaking detection method introduced by Kunz et al. (2009b) is used to explicitly extract anticyclonic and cyclonic wave breaking events from observational data, and its relation with the large-scale tropospheric and stratospheric circulation is studied by means of a composite analysis.

The remainder of this paper is organized as follows: Section 2 describes the data and methods used for the analysis. Section 3 presents anticyclonic and cyclonic wave breaking composites of the temporal and spatial components of the large-scale circulation related to the NAO, while the connection with the stratosphere is investigated in section 4. Conclusions and discussion follow in section 5.

2. Data and methodology

The analysis is based on the 40-yr European Centre for Medium-Range Weather Forecasts (ECMWF) Re-Analysis (ERA-40) dataset, spanning the 45-yr period 1957–2002. Since we want to study (i) the impact of synoptic-scale wave breaking on the NAO and (ii) its connection with the stratospheric polar vortex, extended winter seasons (November–April) are used to include late winter/early spring stratospheric variability (resulting in a total of $45 \times 181 = 8145$ days; neglecting 30 April during leap years). Only data north of 20°N are retained, and daily means are computed for all variables used in this study.

a. Wave breaking detection method

The method for the detection of breaking synoptic-scale Rossby waves in the troposphere is introduced and described in detail by Kunz et al. (2009b). In brief, the method works as follows: first, daily maps of potential vorticity on an upper-tropospheric isentropic surface ($\theta = 320$ K; IPV for short) are calculated as input data and reduced to T42 horizontal resolution to smooth out subsynoptic-scale structures. Then, on this isentrope an individual wave breaking event is defined as a two-dimensional horizontal structure characterized by a reversed (i.e., negative) meridional IPV gradient and is detected and tracked in time by the following three steps:

1) Each individual longitude is searched for meridional IPV reversals with a poleward decrease of IPV by at least one potential vorticity unit (PVU; 1 PVU $\equiv 10^{-6}$ m^2 s^{-1} K kg^{-1}).
2) Different IPV reversals found by step 1 that occur on neighboring longitudes are grouped together and taken as the same wave breaking event if their latitudinal position differs by less than two grid points (about 5° latitude for the T42 Gaussian grid).
3) Two wave breaking events found by step 2 that occur on subsequent days are taken as the same event if they overlap in longitude and latitude. This prevents multiple detection of the same event at consecutive times. The first time of detection is used as the key day for composite purposes, and all events with a lifetime of only one day are discarded to exclude very short lived events that only marginally fulfill the conditions for detection. The location of the breaking wave is defined as the center of the longitude–latitude box, which is bounded by the westernmost and easternmost longitude with an IPV reversal of at least 0.75 PVU and by the southernmost and northernmost latitude of the corresponding IPV maxima and minima, respectively.

Finally, for the classification into anticyclonic (AB) and cyclonic wave breaking (CB) events a kinematic criterion is used based on the zonal stretching deformation $S = (a\cos\phi)^{-1}[u_\lambda - (v\cos\phi)_\phi]$ on the 320-K isentrope, where u and v are the zonal and meridional wind components respectively; λ is longitude; ϕ latitude; a the earth's radius; and indices represent derivatives. This quantity is positive on the trough axis of a typical anticyclonically breaking wave associated with stretching in the zonal direction, whereas the trough of a cyclonically breaking wave is subject to stretching in the meridional direction that makes the trough broader with time and is associated with negative values of S. Hence, the initial stretching S_1, that is, the value of S on the IPV trough at the time of detection, is computed for each individual event, taken on that longitude with the largest IPV reversal. Then, the most distinct AB (CB) events are extracted by selecting those events with an initial stretching above (below) the upper (lower) 30% quantile of the S_1 distribution of all events (for illustration and further details, see Kunz et al. 2009b).

Additionally, for the present study only those events are considered that are detected within the North Atlantic sector (defined as the region north of 20°N between 80°W and 30°E) and occur south of 70°N. Furthermore, all events during the first or last 14 days of each individual season are removed from the analysis to allow for the computation of lagged composites. Then, a total of 1819 wave breaking events are obtained and, on average, an event occurs every 3.8 days. These events have an average lifetime of 7.4 days, 78% of all events are shorter than this average lifetime, and 83% of all events are shorter than 10 days. From these events the most distinct 546 AB and 546 CB events are selected; thus, on average, individual events of either kind occur every 12.6 days. There is virtually no difference between the distributions of lifetimes of AB and CB events and that of all events. On average AB (CB) events are detected at 48°N (52°N). In the zonal direction the locations of the detected events of either kind are spread over a wide range of longitudes, where 50% of all AB events occur to the east of 20°W (average longitude: 22°W) and 50% of all CB events to the west of 33°W (average longitude: 29°W).

The synoptic evolution of these events is illustrated in Fig. 1, where longitude and latitude are measured relative to the point where the breaking wave is detected, and time lags are relative to the time of detection. The large-scale overturning of IPV contours (thick lines) clearly indicates the process of Rossby wave breaking near the tropopause, associated with a reversed meridional IPV gradient. The AB composite exhibits the typical signature of anticyclonic wave breaking with a northeast–southwest tilted IPV trough of an equatorward propagating wave, while the CB composite evolution shows a northwest–southeast tilted trough and a distinct anticyclonic anomaly is generated on the poleward flank of the wave breaking region. Together with the eastward-traveling cyclonic anomaly to the south, a blockinglike circulation pattern is established after lag 0.

These composites closely resemble the findings of Kunz et al. (2009b), where the same method was applied to the output of a simplified general circulation model. However, some features, like the precursory AB event prior to the detected major event and the preexisting blocking pattern in case of CB (as seen in their Fig. 7), are not present in the composites based on the ERA-40 reanalysis owing to larger case-to-case variability in the atmosphere.

b. NAO and stratospheric NAM indices

For the investigation of the impact of wave breaking on the NAO in section 3, the daily NAO index is constructed as follows: (i) The first EOF is computed for monthly mean surface pressure anomalies (w.r.t. the monthly mean climatology) in the North Atlantic sector. (ii) Daily surface pressure anomalies are obtained by subtracting the smoothed daily climatology.[2] (iii) The NAO index (NAOI) time series is then calculated by projection of the North Atlantic sector daily surface pressure anomalies onto the first EOF pattern and is normalized to have zero mean and unit standard deviation.[3] The spatial structure of the NAO is shown in Fig. 2b, and the well-known meridional dipole pattern with a positive (negative) center near the Azores (Iceland) is obtained.

Additionally, the low-frequency (periods >10 days) NAO index (NAOI_L) is constructed similarly to the NAOI, but surface pressure anomalies are filtered by a 19-point Lanczos filter with a cutoff frequency of 10 days before projection. This second NAO index will be used in the context of the stratospheric analysis in section 4.

As a measure of the strength of the lower-stratospheric polar vortex, the low-frequency 50-hPa northern annular mode index NAMI_L is calculated similarly to the NAOI_L but from 50-hPa geopotential height fields instead of surface pressure and data from the entire hemisphere

[2] For the climatology the mean of each individual day of the 181-day seasons is computed and the resulting time series is smoothed by a 61-point Lanczos filter with a cutoff frequency of 60 days (for Lanczos time filtering, see Duchon 1979), including 30 days of October and May to account for the length of the filter.

[3] Fields are weighted by the cosine of latitude ($\cos\phi$) for projection and by $\sqrt{\cos\phi}$ for EOF computation.

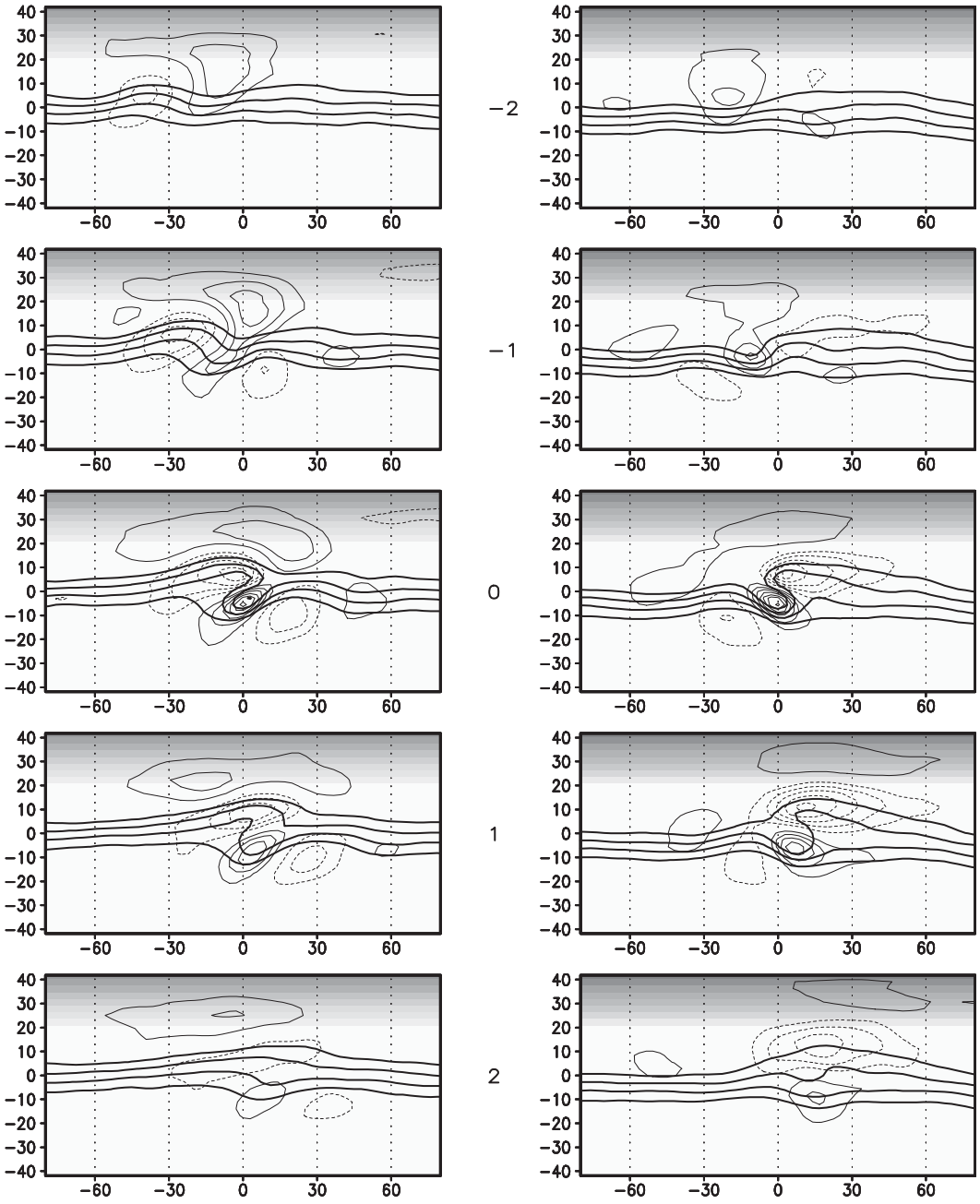

FIG. 1. North Atlantic sector (left) anticyclonic wave breaking (AB) and (right) cyclonic wave breaking (CB) composites of potential vorticity (IPV) anomalies at the $\theta = 320$ K isentropic surface from lag −2 days to +2 days; lags are measured relative to the time of detection of the wave breaking events. Contour interval is 0.2 PVU, the zero contour is omitted, and dashed contours indicate negative values. Thick contours show total IPV at 2, 2.5, 3, and 3.5 PVU. Coordinates are relative longitude and latitude. For some events the high relative latitudes correspond to absolute latitudes beyond 90°N, depending on the latitude of the wave breaking. To indicate this, relative latitudes that occurred for all (zero) events are shaded in white (black).

north of 20°N are used. Figure 2a shows the spatial pattern of the 50-hPa NAM, characterized by a hemispheric-scale high-latitude negative anomaly centered near the pole and a near zonally uniform structure.

3. Impact of wave breaking on the NAO

In this section the relation between North Atlantic synoptic-scale wave breaking and the NAO is investigated

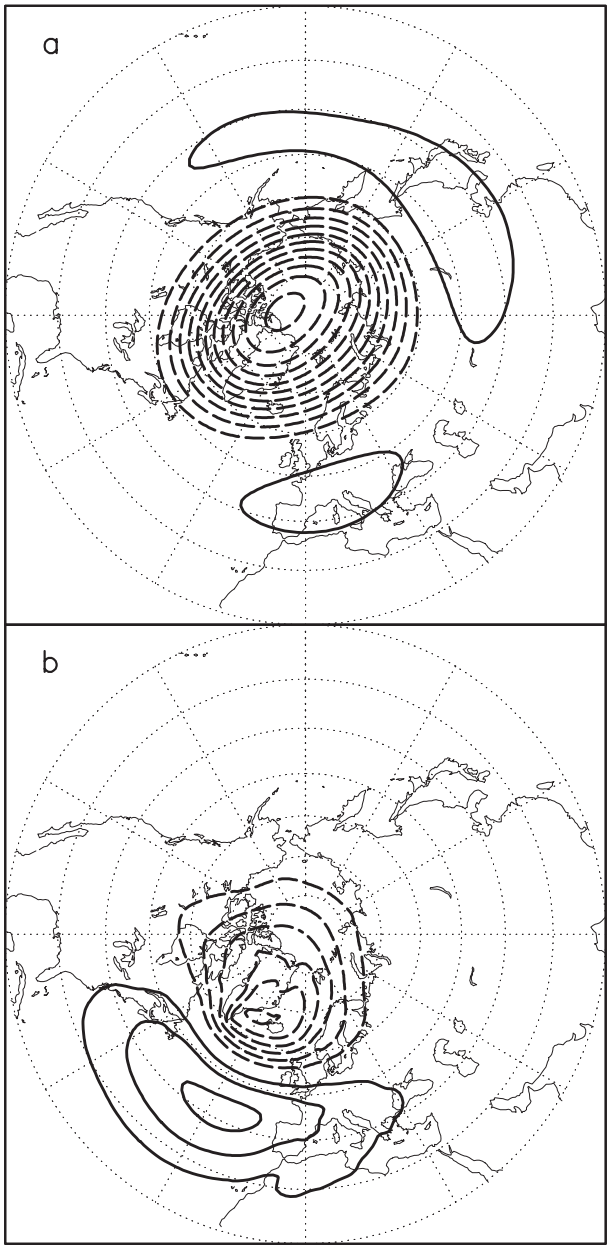

FIG. 2. Regression pattern of (a) low-frequency (periods >10 days) 50-hPa geopotential height anomalies on the low-frequency 50-hPa NAM index ($NAMI_L$) and (b) of unfiltered surface pressure anomalies on the NAO index (NAOI). Contour interval is 30 gpm in (a) and 2 hPa in (b); the zero contour is omitted, and dashed contours indicate negative values.

by means of a composite analysis. Different aspects of the tropospheric circulation are studied in the following.

a. Time evolution of the NAO

First, we focus on the time evolution of the daily NAO index (NAOI) during anticyclonic and cyclonic wave breaking. For this purpose AB and CB composites of the

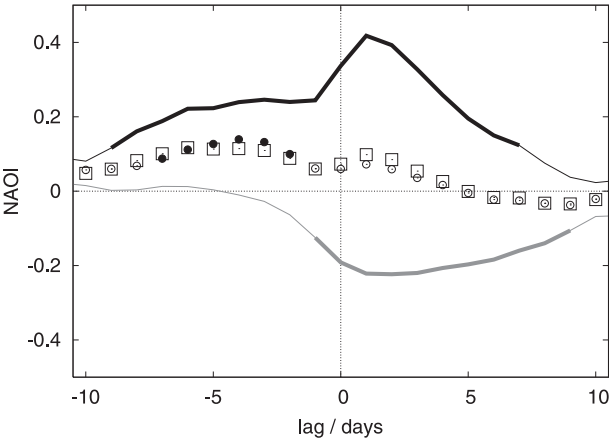

FIG. 3. Wave breaking composites of the NAOI: total composite (circles) including all 1819 wave breaking events; separate composites (lines) for the 30% most distinct AB (black) and CB (gray) events, including 546 events each; and mean (squares) of the AB and CB composites. Thick lines and filled circles indicate statistical significance at the 97.5% level.

NAOI are presented in Fig. 3. Evidently, AB (CB) events occur preferably during the positive (negative) phase of the NAO, indicating a dependence of wave breaking characteristics on the state of the NAO, which in turn is associated with the latitudinal position of the eddy-driven jet in the North Atlantic sector (e.g., Ambaum et al. 2001). At times when AB events are detected (lag 0 in the composite) the normalized NAO index is, on average, at NAOI = +0.34, but at NAOI = −0.19 when CB events are detected.

The wave breaking itself, on the other hand, is found to reinforce the actual phase of the NAO. Specifically, anticyclonic wave breaking leads to a further increase of the NAO index (lag −1 day to +1 day) with its peak value at lag +1 day, while cyclonic wave breaking drives the NAO even deeper into the negative phase until lag +2 days. This confirms the suggestion of Benedict et al. (2004) that AB (CB) events act to drive the positive (negative) phase of the NAO. Thus, the above results suggest the possibility of a positive feedback between the phase of the NAO and synoptic-scale wave breaking in the North Atlantic sector, particularly for the positive phase. This is qualitatively similar to a positive eddy–zonal flow feedback as found in many observational and modeling studies on the interaction between waves and the zonal-mean zonal flow or annular modes (e.g., Yu and Hartmann 1993; Esler and Haynes 1999; Lorenz and Hartmann 2003). Furthermore, the statistically significant NAO signal for cyclonic wave breaking persists until lag +9 days and, thus, 2 days longer than the signal for anticyclonic wave breaking (Fig. 3), although the latter starts at higher values and also attains a larger peak value of NAOI = +0.42 compared to NAOI = −0.22 for CB.

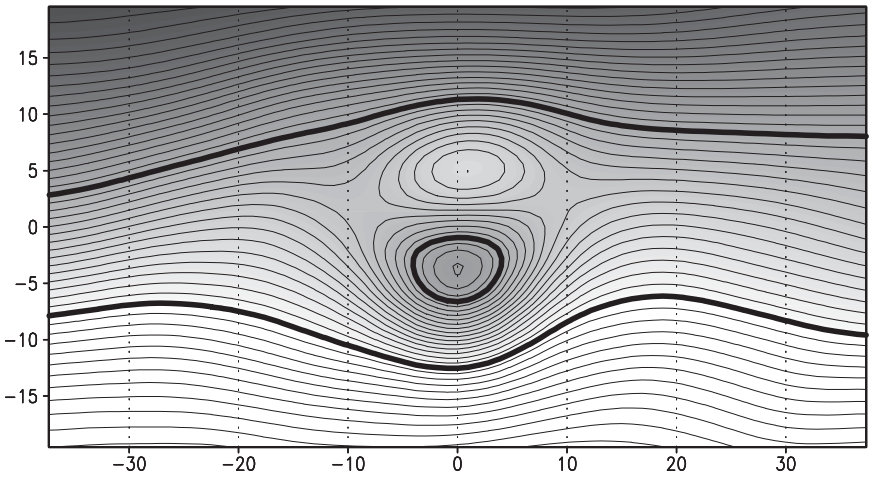

FIG. 4. North Atlantic sector total wave breaking composite (including all 1819 events) of IPV at $\theta = 320$ K at the time of detection (lag 0). Contour interval is 0.1 PVU; thick contours are at 2 and 3.5 PVU; values above 2 PVU are shaded, and darker shading indicates larger values. Coordinates are relative longitude and latitude.

It is also of interest to look at the composite for all wave breaking events (circles in Fig. 3), rather than the 30% most distinct AB and CB events. The fact that this total composite does not systematically differ from and is very close to the mean of the AB and CB composite (squares in Fig. 3) shows that the remaining 40% of all wave breaking events, which are not included in the AB/CB composites, are neither dominated by AB nor by CB events. This, in turn, implies that the total composite can indeed be interpreted as the average evolution of the NAO before and after the occurrence of Rossby wave breaking in general, if solely defined by a reversed meridional IPV gradient without any reference to AB- or CB-like behavior. Figure 4 further confirms that the total of all wave breaking events is not biased toward AB- or CB-like behavior in terms of its IPV signature, as seen in the highly symmetric meridional dipole pattern.

Hence, we can infer from the total composite of the NAO index (Fig. 3, circles) that (i) the process of Rossby wave breaking in general does not drive any distinct NAO anomaly since the total composite of the NAO index does not change near and shortly after the time of detection; (ii) there is a preference for Rossby wave breaking to emerge from the positive phase of the NAO (see the significantly positive total composite at negative lags); and (iii) the significantly positive NAO anomaly preceding AB events is not specifically related to anticyclonic wave breaking but is rather a consequence of point (ii) and of computing the significance for anomalies different from zero (not from the total composite). This might seem contradictory to the successful characterization of the negative phase of the NAO by Woollings et al. (2008) by simply detecting breaking Rossby waves without any distinction between AB and CB. However, the restriction of their analysis to persistent events that, additionally, occur in a spatially more confined key region probably preselects CB events from others in that study.

b. *Spatial structure of the North Atlantic circulation*

We now turn to the spatial structure of the circulation over the North Atlantic during wave breaking. The AB and CB composites of surface pressure, averaged from lag −1 day to +4 days (Figs. 5a and 5b, respectively), clearly reveal meridional dipoles of opposite polarity in the North Atlantic sector, resembling the positive and negative phase of the NAO, respectively. However, the asymmetry between the AB- and CB-composite evolution, found in the temporal component, is reflected not only in the amplitude of the corresponding surface pressure fields but also in the spatial structure itself. Specifically, while the AB surface pressure response very closely resembles the pattern of the NAO (Fig. 2b) at middle and low latitudes, the corresponding CB response pattern exhibits a different orientation of the dipole with a north-northeast–south-southwest tilted axis and its zero line appears at lower latitudes. The AB minus CB composite difference (Fig. 5c) reflects the variability pattern associated with the successive occurrence of AB and CB events in the North Atlantic sector and is spatially correlated at 0.90 (weighted by $\cos\phi$) with the NAO pattern (for comparison, the NAO pattern is correlated at 0.90 and −0.76 with the AB and CB response, respectively).

To further shed light on the dynamics of North Atlantic wave breaking, AB and CB composites of 300-hPa

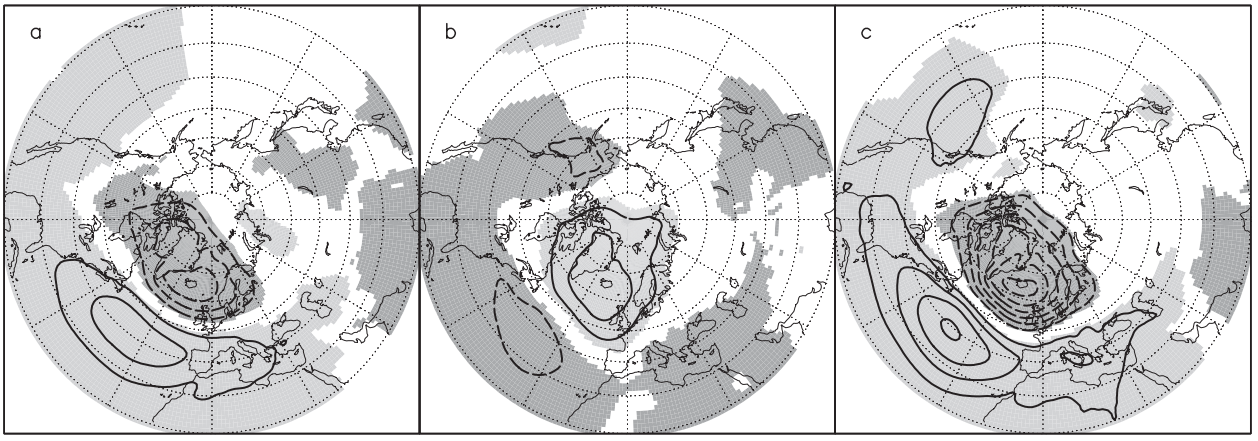

FIG. 5. (a) AB and (b) CB composite of surface pressure anomalies and (c) the difference (a) minus (b); averaged over the period lag −1 . . . +4 days. Contour interval is 1 hPa, the zero contour is omitted, and dashed contours indicate negative values; light (dark) shading indicates statistical significance of positive (negative) anomalies at the 97.5% level.

zonal wind anomalies (w.r.t. the climatology, computed as for surface pressure; see section 2) are presented in Figs. 6a and 6b, again averaged from lag −1 day to +4 days. Since the time mean (November–April) climatological North Atlantic eddy-driven jet (see thin lines in Fig. 6b) is located near 45°N, the positive zonal wind anomaly between 50° and 55°N produced by anticyclonic wave breaking (Fig. 6a) implies a northward shift and strengthening of the jet.[4] Additionally, the negative anomaly to the south between 30° and 35°N increases the anticyclonic shear on the equatorward flank of the jet and also tends to separate it from the North Atlantic subtropical jet near 20°N. In case of cyclonic wave breaking, the negative anomaly near 45°N (Fig. 6b) leads to a weakening of the eddy-driven jet. Both findings closely resemble the response of the North Atlantic jet to variations of the NAO (see Ambaum et al. 2001). Note also that a significantly positive zonal wind anomaly as a response to AB events is found near 30°N between 40° and 140°E (Fig. 6a), indicating a strengthening of the subtropical jet over the Asian continent, while CB events drive a more zonally confined response (Fig. 6b).

The interaction between wave breaking and the mean jets in the North Atlantic sector is further illustrated by composites of the time mean (November–April) climatological 300-hPa horizontal wind speed (Figs. 7a,b)[5] shown in relative longitude and latitude. Two different wind maxima are evident, associated with the eddy-driven jet (at western relative longitudes) and the subtropical jet (at eastern relative longitudes). Note, that the wind maxima are reduced compared to fields in absolute longitude and latitude owing to spatial smoothing since individual wave breaking events occur in different locations. These different spatial distributions of AB and CB occurrences also cause the differences in wind speed between Fig. 7a and Fig. 7b. From the superimposed IPV contours to indicate the position of the breaking wave we can infer that, on average, AB events occur downstream and on the equatorward flank of the eddy-driven jet maximum, while CB events occur downstream and inside or marginally on the poleward flank of the jet. By comparison of Figs. 7a and 7b with Figs. 7c and 7d, where the composites of the total (or instantaneous) wind speed rather than of the climatology are shown, it becomes apparent how anticyclonic wave breaking acts to anomalously separate the two jets in the North Atlantic sector (Fig. 7c), while cyclonic wave breaking tends to merge these jets (Fig. 7d). This is in agreement with Martius et al. (2007) and with the observed jet configurations during the positive and negative phase of the NAO, respectively. Moreover, since composites are shown in relative coordinates, Figs. 7c and 7d indicate that such different jet patterns are inherent features of the two kinds of wave breaking. Together with the correspondence of the two wind speed maxima in each of Figs. 7a and 7b with the North Atlantic eddy-driven and subtropical jet, the above results suggest that the different jet configurations between the two phases of the NAO are simply an average over many individual AB or CB events within the North Atlantic storm-track region. This is in support of the suggestion made by Benedict et al. (2004) and Franzke et al.

[4] It should be noted that the climatological North Atlantic eddy-driven jet does not have a pure zonal orientation but rather a west-southwest–east-northeast axis, in contrast to the almost zonal orientation of the composite zonal wind anomalies.

[5] Similar composites are computed of the daily, that is, seasonally varying, climatology of wind speed rather than of the time mean climatology to account for the timing of individual wave breaking events. However, the results (not shown) are found to closely resemble those shown in Figs. 7a,b.

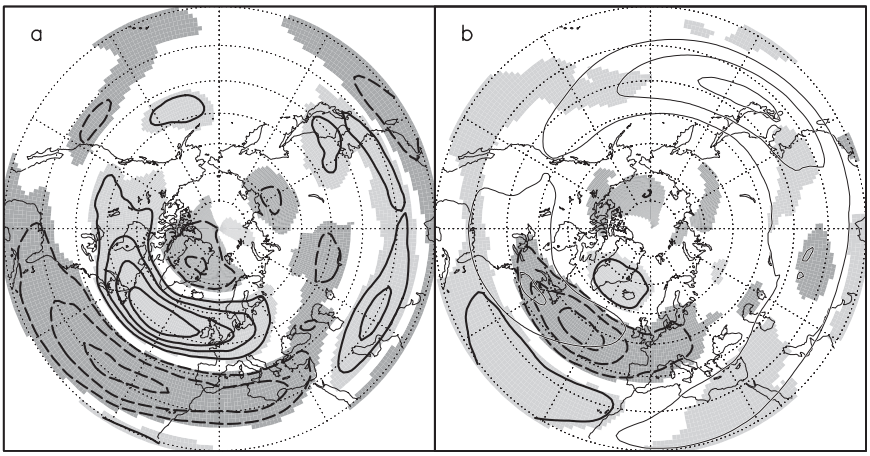

FIG. 6. (a) AB and (b) CB composite of 300-hPa zonal wind anomalies, averaged over the period lag −1 . . . +4 days. Contour interval is 1 m s^{-1}, the zero contour is omitted, and dashed contours indicate negative values; shading as in Fig. 5. Also included in (b) is the time mean (November–April) climatological 300-hPa zonal wind with thin solid contours at 18, 27, and 36 m s^{-1}.

(2004) that the physical entity of the NAO is the remnants of breaking synoptic-scale waves.

Finally, anomalous 300-hPa synoptic-scale momentum fluxes $\overline{u'_H v'_H}$ (w.r.t. the climatology; computed as for surface pressure; see section 2) are shown in Fig. 8, calculated from high-frequency (periods <10 days) zonal and meridional wind components u'_H and v'_H, respectively. During AB (CB) events northward (southward) momentum fluxes across 45°N are found, as expected, since AB (CB) events are associated with equatorward (poleward) synoptic-scale wave propagation during the barotropic decay stage of these waves (see, e.g., Kunz et al. 2009a). These results are dynamically consistent with the zonal wind anomalies in the North Atlantic sector during wave breaking, as seen in Fig. 6 above.

4. Connection with the stratosphere

Next, we investigate the link between North Atlantic synoptic-scale wave breaking and the variability in the lower stratosphere, whereby wave breaking is considered as a potentially relevant component for stratosphere–troposphere interactions. For this purpose, this section concentrates on the relation between wave breaking, different stratospheric circulation patterns, and the NAO.

a. Relation between wave breaking and stratospheric NAM variability

Several studies have identified the NAM as the dominant stratospheric variability mode during winter (e.g., Thompson and Wallace 1998; Baldwin and Dunkerton 1999), which essentially characterizes the strength of the polar night jet, also referred to as the polar vortex. Since tropospheric synoptic-scale waves cannot deeply penetrate into the stratospheric westerlies, as shown by the Charney–Drazin criterion (Charney and Drazin 1961; Andrews et al. 1987), an interaction of these waves can be expected only with the lower stratosphere, rather than with stratospheric levels at greater altitudes.

Therefore, we choose the 50-hPa northern annular mode time series NAMI_L to analyze lower-stratospheric variability. At this level signatures of tropospheric synoptic-scale waves are still observed (Canziani and Legnani 2003, though that study is concerned with the Southern Hemisphere), and a lower level is not chosen to minimize the influence of tropospheric NAM variations. Furthermore, since lower-stratospheric NAM variability is associated with relatively long time scales of about three to four weeks (Baldwin et al. 2003), compared to the troposphere, we use its low-frequency variability component (NAMI_L) throughout this section without loosing important information of the stratospheric flow evolution. For consistency, the low-frequency NAO index (NAOI_L) will be used in the stratospheric composite analysis below.

On average, the 50-hPa NAM index is found to be larger by +0.12 during tropospheric AB than during CB events (at lag 0). This matches the result of the idealized baroclinic wave life cycle simulations by Kunz et al. (2009a) that a stronger (weaker) stratospheric jet can induce anticyclonic (cyclonic) wave breaking in the troposphere. However, the composite difference in the 50-hPa NAM index of the present study is only marginally

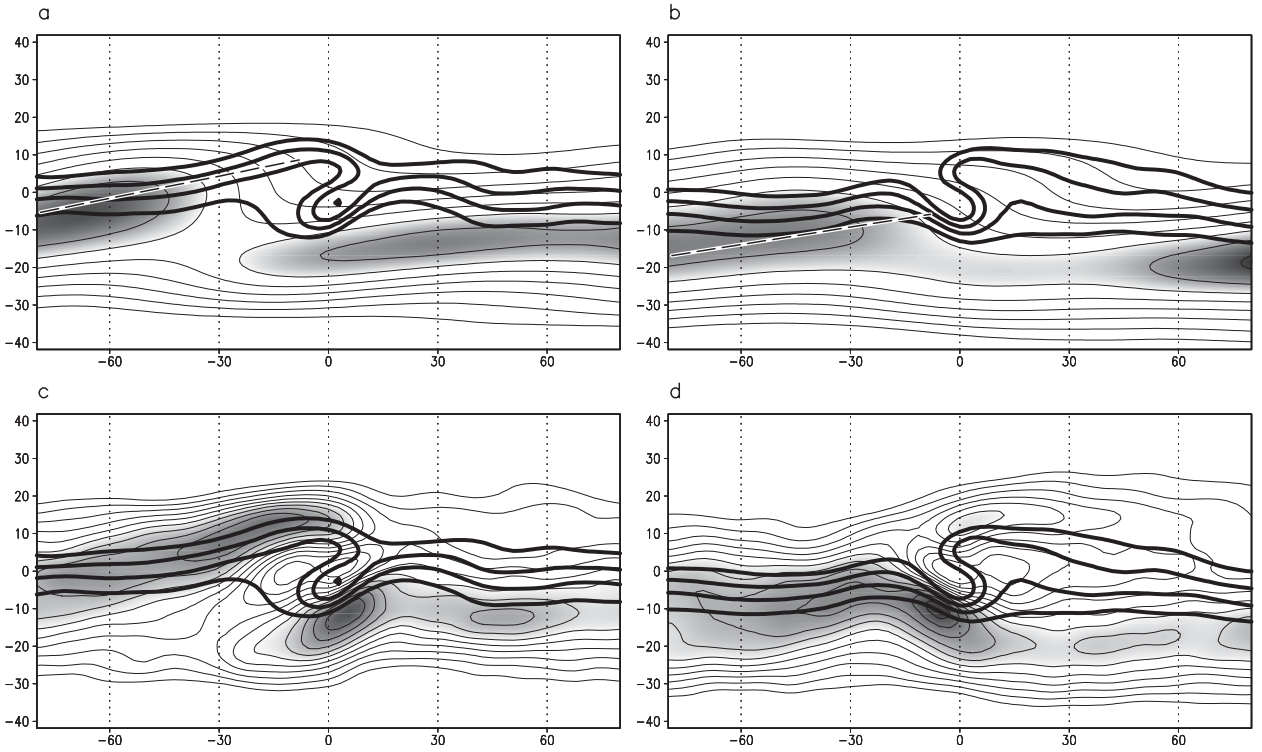

FIG. 7. North Atlantic sector (left) AB and (right) CB composites, shown in relative longitude and latitude, of (top) the time mean (November–April) climatological 300-hPa horizontal wind speed and (bottom) the total, or instantaneous, 300-hPa horizontal wind speed, at lag 0 (the time of detection). Contour interval is 1.5 m s^{-1}; lowest contour is at 13.5 m s^{-1} in (a) and (b) and at 19.5 m s^{-1} in (c) and (d); values above 21 m s^{-1} in (a) and (b) and above 27 m s^{-1} in (c) and (d) are shaded; darker shading indicates larger values. Thick contours show total IPV on the 320-K isentrope at 2, 2.5, 3, and 3.5 PVU. The straight dashed lines in (a) and (b) mark the approximate position of the axis of the eddy-driven jet.

significant at the 97.5% confidence level—not surprisingly, since the internal synoptic variability of the troposphere is large compared to stratospheric influences (see, e.g., Charlton et al. 2004) and both kinds of wave breaking can certainly occur during either phase of the stratospheric NAM. Thus, it is also reasonable to study the downward influence of stratospheric perturbations on the tropospheric circulation.

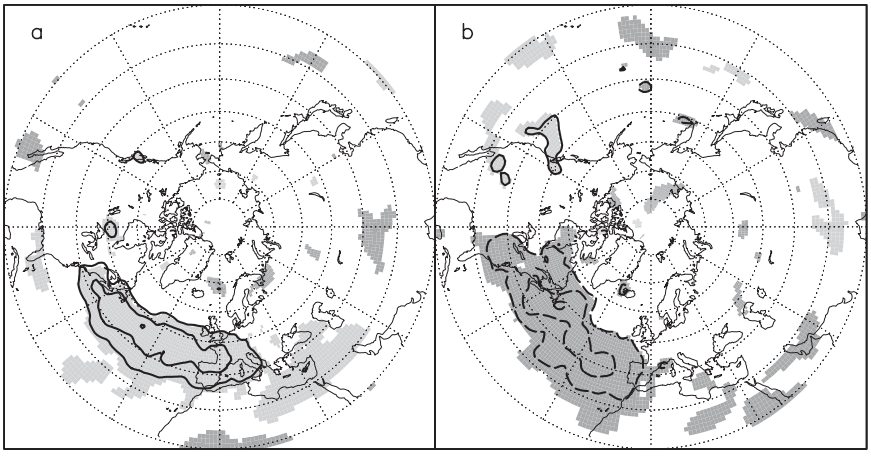

FIG. 8. As in Fig. 6, but for anomalies of 300-hPa momentum fluxes $\overline{u'_H v'_H}$ due to synoptic-scale (periods <10 days) variations, contour interval is 5 m^2 s^{-2}; averaged over the period lag −1 . . . +4 days.

TABLE 1. Onset dates of the 29 weak vortex (WV) events detected from the 50-hPa NAM time series ($NAMI_L$). For comparison, central dates of corresponding sudden stratospheric warming (SSW) events as detected at the 10-hPa level by Charlton and Polvani (2007) from the ERA-40 dataset are also included [SSW events that are not found in the ERA-40 dataset by their detection algorithm but only in the National Centers for Environmental Prediction–National Center for Atmospheric Research (NCEP–NCAR) reanalysis are marked by an asterisk].

Event	WV, onset date	Corresponding SSW, central date
1	26 Jan 1958	31 Jan 1958
2	22 Nov 1958	30 Nov 1958*
3	26 Dec 1959	15 Jan 1960
4	9 Dec 1960	—
5	18 Mar 1961	—
6	28 Jan 1963	28 Jan 1963
7	20 Mar 1964	—
8	5 Dec 1965	16 Dec 1965
9	19 Feb 1966	23 Feb 1966
10	4 Jan 1968	7 Jan 1968
11	23 Dec 1968	28 Nov 1968
12	20 Dec 1969	1 Jan 1970
13	14 Jan 1971	18 Jan 1971
14	16 Feb 1973	31 Jan 1973
15	24 Mar 1974	—
16	19 Mar 1975	—
17	23 Dec 1976	9 Jan 1977
18	28 Feb 1981	4 Mar 1981
19	10 Mar 1984	24 Feb 1984
20	27 Dec 1984	1 Jan 1985
21	21 Jan 1987	23 Jan 1987
22	29 Nov 1987	7 Dec 1987
23	18 Nov 1996	—
24	29 Dec 1997	—
25	30 Dec 1998	15 Dec 1998
26	26 Feb 1999	26 Feb 1999
27	12 Dec 2000	—
28	3 Feb 2001	11 Feb 2001
29	26 Dec 2001	30 Dec 2001

b. *Response of the NAO to stratospheric weak vortex episodes*

Many studies investigate the tropospheric response to strong as well as weak stratospheric polar vortex episodes (e.g., Baldwin and Dunkerton 2001; Perlwitz and Graf 2001; Charlton et al. 2004). From a dynamical perspective, however, anomalously strong polar vortex conditions should rather be viewed as the unperturbed state, while weak vortex conditions reflect a highly disturbed stratospheric circulation in the sense of a displaced, stretched, or even split polar vortex, as observed during sudden stratospheric warmings (e.g., Charlton and Polvani 2007). These sudden stratospheric warmings, which are triggered by pulses of upward planetary wave propagation, represent the most dramatic synoptic events observed in the stratosphere, usually associated with a rapid distortion or disruption of the polar vortex followed by a gradual recovery over the subsequent weeks.

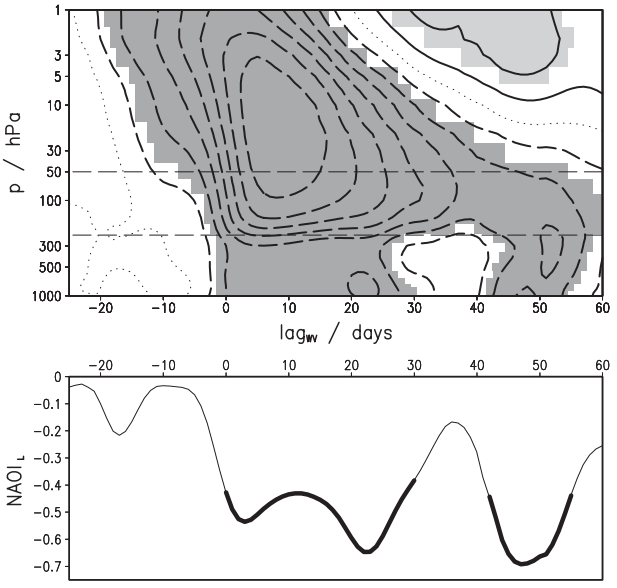

FIG. 9. Weak stratospheric vortex composite (see text for details) of (top) the NAM index $NAMI_L$ between 1 and 1000 hPa and (bottom) the low-frequency NAO index $NAOI_L$; lags are measured relative to the weak vortex event onset day. Contour interval (top) is 0.25, the zero contour is dotted, and dashed contours indicate negative values. Statistical significance is indicated by shading (top, as in Fig. 5) and thick lines (bottom, as in Fig. 3). The 50-hPa level where the weak vortex events are detected and the midlatitude tropopause near 210 hPa (~11 km) are marked by thin horizontal dashed lines.

Accordingly, we focus on stratospheric perturbations characterized by persistent negative NAM anomalies and define a weak vortex event as an episode during which the 50-hPa NAM index $NAMI_L < -1$ standard deviation for at least 14 days. If two events (during the same winter season) are separated by less than 35 days, the weaker event is discarded to prevent multiple detection of the same event. With these criteria, a total of 29 weak vortex events are detected. All onset dates, defined as the first day of an event, are listed in Table 1 together with corresponding sudden stratospheric warmings as detected by Charlton and Polvani (2007). The fact that most of our weak vortex events are found to correspond to a sudden stratospheric warming (as detected at the 10-hPa level) demonstrates the close relation between these two different definitions of stratospheric perturbations.

The weak vortex composite evolution is shown in Fig. 9, where the NAM index at all other pressure levels of the ERA-40 dataset (computed similarly to the 50-hPa NAM index $NAMI_L$; see section 2b) is

included in the upper panel to illustrate the vertical structure of these events. Evidently, a clear downward propagation signature through the whole depth of the stratosphere down to the earth's surface is present, in a similar fashion as shown by Baldwin and Dunkerton (2001). To avoid any confusion with lags related to wave breaking events, the subscript WV is added to all lags that refer to the weak vortex composite. At 1 hPa the NAM index passes −1 standard deviation already at lag_{WV} −7 days, and the most persistent statistically significant negative anomaly is observed in the lowermost stratosphere at 100 hPa that lasts until 60 days after the 50-hPa weak vortex onset day (lag_{WV} +60 days).[6]

The most interesting feature, however, is the significant tropospheric response until about eight weeks after the event onset, which is seen most clearly in the low-frequency NAO index (NAOI_L, lower panel of Fig. 9). A significant negative NAOI_L anomaly appears from lag_{WV} 0 to +30 days and from lag_{WV} +42 days to +55 days. Here, the reduced response between lag_{WV} +30 days and +42 days is probably due to the small sample of only 29 weak vortex events during the 45 analyzed winter seasons and might vanish for an increased sample size. Note that the time scale of the tropospheric response that extends over several weeks (much longer than the synoptic time scale) underlines the relevance of dynamical stratosphere–troposphere coupling for tropospheric intraseasonal low-frequency variability. Finally, the very similar behavior during weak vortex episodes of the NAO index to that of the tropospheric NAM index supports the findings of other studies that (i) the tropospheric response to stratospheric NAM perturbations is reflected predominantly in the NAO (e.g., Baldwin et al. 1994) and (ii) a close relationship exists between the NAO and the tropospheric NAM (Wallace 2000; Ambaum et al. 2001; Vallis et al. 2004; Feldstein and Franzke 2006). In fact, in our analysis the low-frequency NAO index (NAOI_L) and 1000-hPa NAM index time series are correlated at 0.88.

c. *Wave breaking during stratospheric weak vortex episodes*

Returning now to the relation between North Atlantic wave breaking and stratospheric perturbations, we analyze their effect on the frequencies of AB and CB events in the troposphere during weak vortex episodes. Since AB and CB events are found to have an opposite effect on the NAO we compute the difference between the number of detected AB and CB events $N_{\text{AB}} - N_{\text{CB}}$ by counting events during 21-day periods to obtain a smoothed result. Small changes of the averaging period do not substantially modify the results, though for considerably shorter averaging periods the resulting time series becomes very noisy. The weak vortex composite of this difference is shown in Fig. 10, where lags refer to the center of each individual 21-day period. On average, 1.67 AB and 1.67 CB events are detected per 21 days. Accordingly, the right axis in Fig. 10 specifies the relative deviation of $N_{\text{AB}} - N_{\text{CB}}$ per 21 days from the average, that is, the left axis divided by 1.67. Significances are determined by a blocked bootstrapping approach. Specifically, the same number of nonoverlapping 21-day periods as used for a given lag is selected randomly from the time series. Repeating this procedure for 10 000 times, the upper and lower 97.5% quantiles of the $N_{\text{AB}} - N_{\text{CB}}$ distribution are obtained and used as significance thresholds.

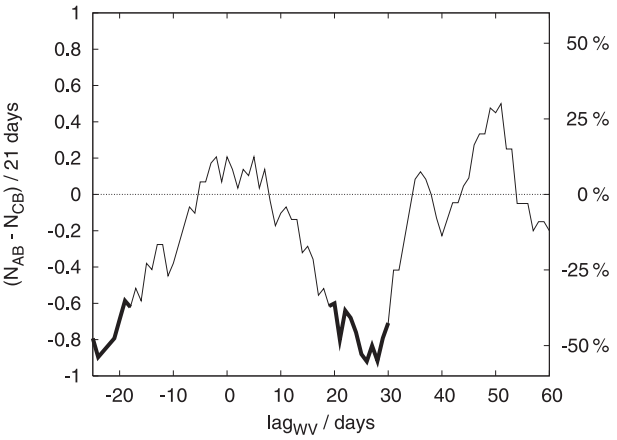

FIG. 10. Weak vortex composite of the difference between the number of AB and CB events $N_{\text{AB}} - N_{\text{CB}}$ per 21 days (left axis); lags refer to the central day of each individual 21-day period. Thick lines indicate statistical significance at the 97.5% level. The right axis relates the number differences to the average number of AB or CB events per 21 days.

As can be seen from Fig. 10, increasingly more CB than AB events are detected during weak vortex events following lag_{WV} 0, until a significant negative anomaly appears from lag_{WV} +19 days to +30 days with up to 55% more CB or less AB events, respectively. This coincides with the negative NAO response period from lag_{WV} 0 to +30 days. Subsequently, the difference of AB and CB occurrences rapidly drops to zero until lag_{WV} +34 days, almost simultaneously with a reduction of the NAO response until lag_{WV} +36 days. These results further confirm the close relation between North Atlantic synoptic-scale wave breaking and the NAO.

Furthermore, although the late NAO response (lag_{WV} +42 days to +55 days) is stronger than that during the

[6] Note that the onset date of a few events occurs less than 60 days before the end of the season. Therefore, a smaller number of events is used for composite and significance computation beyond lag_{WV} +50 days, and only 24 events enter the analysis at lag_{WV} +60 days.

earlier period (lag_{WV} 0 to +30 days), it is not accompanied by any significant signal in wave breaking frequencies. Since, additionally, the negative NAM anomaly in the lower stratosphere is already largely reduced during the later period, the results may suggest that during weak vortex episodes North Atlantic wave breaking characteristics respond primarily to the lower-stratospheric NAM and only secondarily to the NAO. However, another contribution to the lack of statistical significance during the late NAO response may be the relatively short time scale of that episode compared to the 21-day period used to estimate wave breaking frequencies. Finally, significantly more CB than AB events are detected about three weeks prior to weak vortex events (lag_{WV} −18 days and before). However, it is inconclusive how this is related to the onset of weak vortex episodes.

The above results hint at the possibility that (i) tropospheric baroclinic disturbances are, to some extent, modulated (in terms of their wave breaking characteristics) by variations of the lower-stratospheric flow conditions and (ii) the aggregated effect of these changes to individual synoptic systems, in turn, projects onto the NAO at the earth's surface (as also suggested by Charlton et al. 2004, though the results of that study are discussed in the tropospheric NAM framework rather than the NAO). Note that the choice of the 50-hPa level for the detection of the weak vortex events does not imply that it is this level that may influence tropospheric wave breaking processes. It is rather plausible that tropospheric baroclinic systems respond to persistent flow anomalies near the tropopause. Finally, it should be pointed out that the above discussion does not rule out alternative mechanisms for dynamical stratosphere–troposphere coupling, as mentioned in the introduction, in particular, since the above mechanism has not yet been thoroughly quantified.

d. Relation between wave breaking and nonannular stratospheric variability

The suggested coupling mechanism, that is, the direct modulation of synoptic systems by lower-stratospheric flow conditions, implies a particular sensitivity of the NAO to variations of the stratospheric flow above the North Atlantic sector rather than coherent hemispheric-scale variability as described by the 50-hPa NAM. Furthermore, not every weak vortex event is followed by a response in the troposphere, as shown, for example, by Baldwin and Dunkerton (2001) for the winter 1998/99. Additionally, weak vortex events are closely related to sudden stratospheric warmings (as shown in section 4c above; see also Table 1), and sudden stratospheric warmings exhibit a large variety of lower-stratospheric flow patterns associated with polar vortex displacements and/or splits (e.g., Matthewman et al. 2009), leading to either an increase or a reduction of the associated negative zonal flow anomaly above the North Atlantic storm-track region. Thus, the specific flow evolution in the lower stratosphere during an individual weak vortex event may control the strength of the associated NAO response, depending on the flow configuration above the North Atlantic sector and the subsequent changes to tropospheric wave breaking characteristics.

Accordingly, we finally compute the residual 50-hPa geopotential height anomalies z'_{res}, that is, the low-frequency 50-hPa geopotential height anomaly fields $z'_L(\mathbf{x}, t)$ minus the coherent hemispheric-scale variability given by the 50-hPa NAM index NAMI_L, defined as

$$z'_{\text{res}}(\mathbf{x}, t) = z'_L(\mathbf{x}, t) - z'_{\text{NAM}}(\mathbf{x}, t), \tag{1}$$

where $z'_{\text{NAM}}(\mathbf{x}, t) = \text{NAMI}_L(t)\text{NAM}(\mathbf{x})$ with the 50-hPa NAM pattern $\text{NAM}(\mathbf{x})$ given by the regression pattern shown in Fig. 2a. Then the connection between tropospheric wave breaking and the nonhemispheric-scale variability in the stratosphere is demonstrated by means of AB and CB composites in Fig. 11.

The residual 50-hPa signature during AB events (Fig. 11c), averaged from lag −4 days to +5 days, w.r.t. wave-breaking detection, indicates a cyclonic anomaly near Iceland and, thus, increased westerly flow above the North Atlantic storm track at midlatitudes, while an even stronger anomaly of opposite sign is observed during CB events (Fig. 11d), contributing to anomalous easterly flow above the tropospheric storm track. Additional inspection of the residual 50-hPa heights up to two weeks prior to CB events (Fig. 11b), averaged from lag −14 days to −5 days, reveals a lower-stratospheric evolution that resembles a polar vortex split and subsequent occurrence of displaced vortex fragments as observed during sudden stratospheric warming events. Note, however, that the composite includes all wave breaking events (e.g., it is not restricted to weak vortex episodes), and thus only part of these patterns may, in fact, reflect lower-stratospheric signatures of sudden stratospheric warmings. On the other hand, before and during AB events (Figs. 11a and 11c) the residual 50-hPa heights exhibit a tripole pattern with an anticyclonic anomaly near the pole and adjacent cyclonic anomalies over the northern North Atlantic and over northeast Siberia. This indicates a horizontally stretched vortex, approximately along the 35°W–145°E axis, such that lower-stratospheric zonal winds are increased above the North Atlantic storm-track region.

Similar wave breaking composites of the residual 50-hPa geopotential height anomalies restricted to events that occur during weak vortex episodes, however, do not

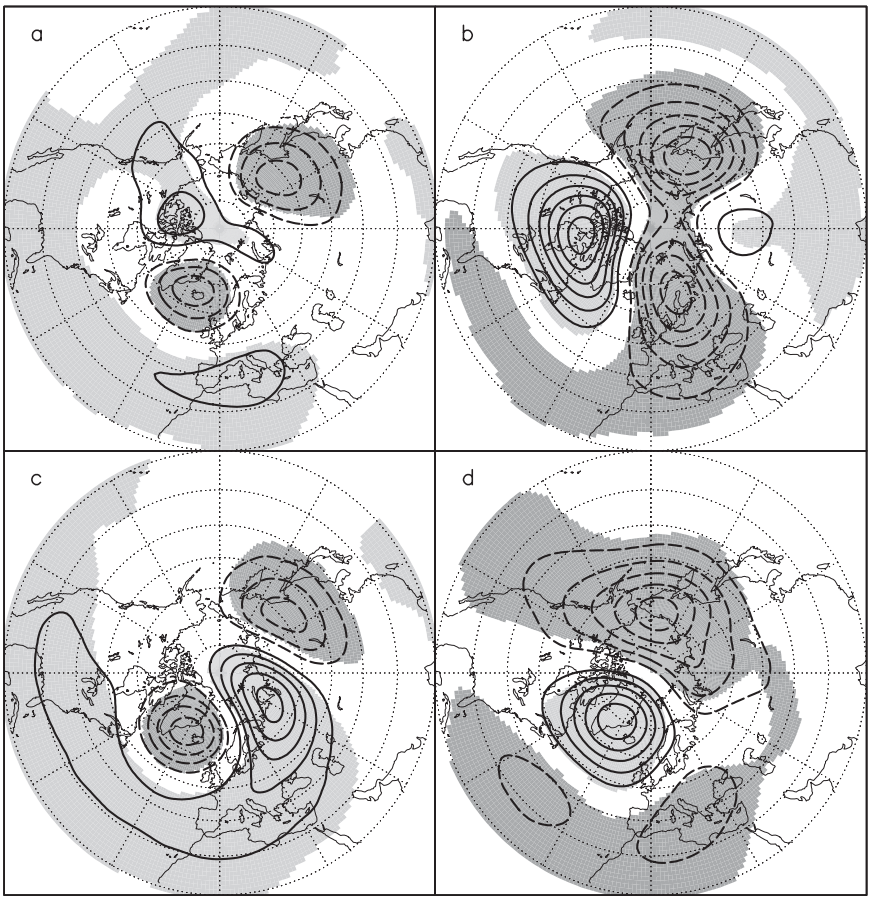

FIG. 11. (left) AB and (right) CB composite of residual 50-hPa geopotential height anomalies z'_{res} (i.e., geopotential height minus NAM variability; see text for details) averaged over the period (top) lag $-14 \ldots -5$ days and (bottom) lag $-4 \ldots +5$ days. Contour interval is 5 gpm, zero contour omitted, and dashed contours indicate negative values; shading as in Fig. 5.

yield statistically significant results owing to the small number of only 29 weak vortex events. Thus, a further extension of a similar analysis will be done in a future study investigating long-term integrations of a stratosphere-resolving general circulation model.

5. Discussion and conclusions

This observational study investigates the impact of North Atlantic synoptic-scale wave breaking on the NAO and its connection with the stratosphere, as derived from the ERA-40 reanalysis. Wave breaking events are detected from daily maps of potential vorticity at the 320-K isentropic surface, using a kinematic criterion for classification into anticyclonic (AB) and cyclonic wave breaking (CB). By restricting the analysis to the North Atlantic sector, a total of 1819 wave breaking events is obtained from 45 extended winter seasons (November–April) during the 1957–2002 analysis period. Then, the 30% most distinct AB and CB events are selected (546 events each) from which a North Atlantic wave breaking climatology is constructed.

First, the relation between North Atlantic synoptic-scale wave breaking and the NAO is investigated by means of a composite analysis (section 3). Specifically, wave breaking composites are compiled of the time evolution of the NAO, anomalies of surface pressure and of 300-hPa zonal wind, and synoptic-scale momentum fluxes. The main conclusions of this part are the following:

- Anticyclonic (cyclonic) wave breaking is intimately linked with and drives/reinforces the positive (negative) phase of the NAO, as previously suggested by Benedict et al. (2004). The positive (negative) phase of the NAO, in turn, favors the occurrence of AB (CB) events. Thus, the results suggest the possibility of a positive feedback between the two kinds of wave breaking and either phase of the NAO.

- Wave breaking in general without any reference to AB- or CB-like behavior, however, does not have an effect on the NAO, though it occurs preferably during its positive phase.
- An asymmetry between the different kinds of wave breaking exists in the temporal as well as spatial component in the sense that anticyclonic wave breaking is associated with a shorter and stronger signal of the NAO compared to a slightly more persistent and weaker signal to cyclonic wave breaking.
- AB (CB) occurrences are associated with northward (southward) synoptic-scale momentum fluxes across 45°N. Consistently, the North Atlantic eddy-driven jet is strengthened and shifted poleward during AB events, while it is weakened during CB. Additionally, AB acts to separate the North Atlantic eddy-driven jet from the subtropical jet, while CB tends to merge these jets. These changes to the jet closely resemble the NAO-related changes of the zonal wind in the North Atlantic sector found by Ambaum et al. (2001).
- North Atlantic AB events are associated with a strengthened subtropical jet over the Asian continent, while CB events drive a more zonally confined response within the North Atlantic sector. The different zonal extent of the response to AB and CB is also in agreement with Kunz et al. (2009b).

Regarding the wave breaking detection method it is important to note that, since the concept of anticyclonic and cyclonic wave breaking is motivated by highly idealized baroclinic wave life cycle simulations, it will hardly be possible to construct any method that identifies either kind of wave breaking for certain when applied to real atmospheric data. As is familiar to any synoptician, daily tropopause charts exhibit a large variety of different IPV signatures as a result of ubiquitous nonlinear interactions of the baroclinic disturbances with waves of different scales and with the time mean flow, in contrast to the highly simplified conditions in idealized life cycle simulations. Since real baroclinic waves are typically observed to grow and propagate on strongly nonzonal and time-varying background flows, it is sometimes even impossible to decide subjectively whether a certain feature should be classified as anticyclonic or cyclonic wave breaking. To this end, we repeat the statement of McIntyre and Palmer (1985) that the concept of breaking Rossby waves does not refer to any automatically recognizable shape. Thus, it is reasonable, and probably inevitable, to restrict the analysis of anticyclonic and cyclonic wave breaking to the most distinct AB and CB events, underlining the plausibility of the approach taken for the presented analysis.

The results of Benedict et al. (2004) indicate that, in addition to a major AB event over the North Atlantic, a second precursory AB event occurs near the North American west coast during the onset of the positive phase of the NAO, yet the wave breaking analysis of the present study is confined to the North Atlantic sector. However, Benedict et al. (2004) show that these two AB events do not drive the NAO independently, but rather it is their interaction that establishes the positive phase of the NAO (see also Kunz et al. 2009a for a discussion of this interaction in a related model study). From this it is plausible to restrict our analysis to North Atlantic AB events and to exclude those precursory AB events that occur to the west of our North Atlantic sector as defined in section 2.

The specific isentropic level used for the detection of wave breaking, at $\theta = 320$ K, also appears to be a reasonable choice in the sense that the total composite of IPV (Fig. 4) does not reveal any bias toward either kind of wave breaking, reflected in the highly symmetric IPV dipole pattern. Note, however, that this is not an inherent result of the method itself. The analysis of Martius et al. (2007) demonstrates that the frequency of AB (CB) events is maximized on higher (lower) isentropic levels in the troposphere, also in the North Atlantic sector. Therefore, changing the isentropic level in our analysis significantly to higher or lower values will indeed result in a bias toward either AB- or CB-like behavior; the same could happen if the analysis is applied to an area (or time episode) that is dominated by the occurrence of one particular kind of wave breaking.

Strong and Magnusdottir (2008) demonstrate that either kind of wave breaking can have both positive and negative projection onto the NAO pattern, depending on the latitudinal position. Specifically, they objectively define regions where AB or CB, respectively, most effectively excites the positive or negative phase of the NAO. They find that, over the North Atlantic, AB occurs most frequently in almost the same region where it excites the positive phase of the NAO. By contrast, the regions of most frequent CB, over the North Atlantic, and those where CB excites the negative phase of the NAO do only partly coincide, with some CB activity in regions where it does not excite the NAO at all or even the opposite phase. These results of Strong and Magnusdottir (2008) may explain part of our finding that AB is associated with a stronger signal in the NAO compared to CB since the composite of the NAO index (Fig. 3) does not account for the latitudinal position of individual events.

The second part of the present study (section 4) focuses on the link between North Atlantic synoptic-scale

wave breaking and the variability in the lower stratosphere together with related variations of the NAO. Lower-stratospheric variability is characterized by (i) the 50-hPa northern annular mode (NAM) and (ii) the residual, that is, the nonannular variability at 50 hPa. Here, we can draw the following main conclusions:

- On average the 50-hPa NAM index attains larger values during tropospheric AB events than during CB (though this difference is only marginally significant). This result is consistent with the idealized baroclinic wave life cycle study by Kunz et al. (2009a), where anticyclonic wave breaking is induced by a strengthened stratospheric polar night jet.
- Stratospheric weak vortex events, closely related to sudden stratospheric warmings, exhibit a downward propagation signature from upper-stratospheric levels near the stratopause down to the earth's surface (similar to the result of Baldwin and Dunkerton 2001) and are followed by a statistically significant negative NAO response that lasts for up to 55 days after the weak vortex event onset.
- During weak vortex episodes increasingly more CB than AB events are observed in the troposphere concurrently with the negative NAO response, and this (significant) difference is maximized about four weeks after the weak vortex onset. Closer inspection of this analysis hints at the possibility that tropospheric wave breaking characteristics during lower-stratospheric weak vortex events are influenced directly by the lower-stratospheric NAM. The small number of only 29 weak vortex events detected during the 45 extended winter seasons, however, limits the interpretation of the above results due to reduced statistical significance.
- Tropospheric wave breaking is also linked to nonannular variations in the lower stratosphere, indicating the preferred occurrence of AB (CB) events below westerly (easterly) flow anomalies confined above the North Atlantic storm-track region. Specifically, the residual 50-hPa geopotential height anomalies prior to and during AB events characterize a horizontally stretched stratospheric polar vortex, approximately along the 35°W–145°E axis, while for CB the evolution is suggestive of a vortex split signature (as observed during sudden stratospheric warmings) with a specific configuration such that a northern North Atlantic anticyclone leads to anomalous easterly flow above the North Atlantic storm track.

Hence, the findings of this study suggest that North Atlantic synoptic-scale wave breaking is one key component for stratosphere–troposphere interactions (as suggested by previous studies; see Baldwin and Dunkerton 1999, 2001; Baldwin et al. 2003; Kushner and Polvani 2004; Charlton et al. 2004; Wittman et al. 2004, 2007; Kunz et al. 2009a), in particular for the response of the NAO to perturbations of the polar vortex, as observed during weak vortex episodes or, similarly, sudden stratospheric warmings. Furthermore, the results indicate a sensitivity of tropospheric wave breaking to nonannular variability patterns in the lower stratosphere, which represent distortions of the polar vortex. From this we may speculate that the specific configuration of the nonannular lower-stratospheric flow evolution during weak vortex episodes controls, to some extent, the strength of the associated NAO response.

Different stratospheric flow configurations during sudden stratospheric warming events may, at first order, be associated with the two dynamically different event types characterized by either a vortex displacement or vortex split, both of which are concisely presented and compared by Charlton and Polvani (2007). Although they conclude that there is only little difference in the averaged (i.e., hemispheric scale) tropospheric response to either type of warming, they find significant differences on a more regional scale, particularly in the Atlantic and in the Pacific sector as well as over Siberia. However, the distinction between these two types of sudden stratospheric warmings is motivated by their different dynamical evolution in the stratosphere and, thus, may not capture the most important differences in the context of the coupling with the troposphere. Matthewman et al. (2009) further investigate both types of warmings and, though the overall stratospheric vortex structure is found to be rather locked to the earth's topography, they note that there is considerable variability of the vortex structure at low stratospheric levels among individual vortex split events. These findings indicate that the flow at lower-stratospheric levels contains considerable variability that may control the strength of the tropospheric response as suggested above and in section 4d.

To further confirm this idea, however, a larger sample of weak vortex events is needed to obtain improved statistics. Then additional stratospheric variability modes may be extracted to characterize the differences between weak vortex episodes with strong and with weak tropospheric (NAO) response. This prompts us to apply a similar analysis to the output of a stratosphere-resolving general circulation model in a future study. Another important issue in this context will be the exact quantification of this and of alternative mechanisms for dynamical stratosphere–troposphere coupling to allow for an estimation of its potential relevance for

extended-range intraseasonal weather forecasts as well as climate change.

Acknowledgments. This work was funded by the Deutsche Forschungsgemeinschaft, project SFB-512 ''Cyclones and the North Atlantic Climate System.'' The Model and Data group at the Max Planck Institute for Meteorology in Hamburg is acknowledged for providing the ERA-40 dataset.

REFERENCES

Abatzoglou, J. T., and G. Magnusdottir, 2006: Opposing effects of reflective and nonreflective planetary wave breaking on the NAO. *J. Atmos. Sci.,* **63,** 3448–3457.

Ambaum, M. H. P., and B. J. Hoskins, 2002: The NAO troposphere–stratosphere connection. *J. Climate,* **15,** 1969–1978.

——, ——, and D. B. Stephenson, 2001: Arctic Oscillation or North Atlantic Oscillation. *J. Climate,* **14,** 3495–3507.

Andrews, D. G., J. R. Holton, and C. B. Leovy, 1987: *Middle Atmosphere Dynamics*. Academic Press, 489 pp.

Baldwin, M. P., and T. J. Dunkerton, 1999: Propagation of the Arctic Oscillation from the stratosphere to the troposphere. *J. Geophys. Res.,* **104,** 30 937–30 946.

——, and ——, 2001: Stratospheric harbingers of anomalous weather regimes. *Science,* **294,** 581–584.

——, X. Cheng, and T. J. Dunkerton, 1994: Observed correlations between winter-mean tropospheric and stratospheric circulation anomalies. *Geophys. Res. Lett.,* **21,** 1141–1144.

——, D. B. Stephenson, D. W. J. Thompson, T. J. Dunkerton, A. J. Charlton, and A. O'Neill, 2003: Stratospheric memory and skill of extended-range weather forecasts. *Science,* **301,** 636–640.

Benedict, J. J., S. Lee, and S. B. Feldstein, 2004: Synoptic view of the North Atlantic Oscillation. *J. Atmos. Sci.,* **61,** 121–144.

Canziani, P. O., and W. E. Legnani, 2003: Tropospheric–stratospheric coupling: Extratropical synoptic systems in the lower stratosphere. *Quart. J. Roy. Meteor. Soc.,* **129,** 2315–2329.

Charlton, A. J., and L. M. Polvani, 2007: A new look at stratospheric sudden warmings. Part I: Climatology and modeling benchmarks. *J. Climate,* **20,** 449–469.

——, A. O'Neill, W. A. Lahoz, and A. C. Massacand, 2004: Sensitivity of tropospheric forecasts to stratospheric initial conditions. *Quart. J. Roy. Meteor. Soc.,* **130,** 1771–1792.

Charney, J. G., and P. G. Drazin, 1961: Propagation of planetary-scale disturbances from the lower into the upper atmosphere. *J. Geophys. Res.,* **66,** 83–109.

Duchon, C. E., 1979: Lanczos filtering in one and two dimensions. *J. Appl. Meteor.,* **18,** 1016–1022.

Esler, J. G., and P. H. Haynes, 1999: Baroclinic wave breaking and the internal variability of the tropospheric circulation. *J. Atmos. Sci.,* **56,** 4014–4031.

Feldstein, S. B., 2000: The timescale, power spectra, and climate noise properties of teleconnection patterns. *J. Climate,* **13,** 4430–4440.

——, 2003: The dynamics of NAO teleconnection pattern growth and decay. *Quart. J. Roy. Meteor. Soc.,* **129,** 901–924.

——, and C. Franzke, 2006: Are the North Atlantic Oscillation and the northern annular mode distinguishable? *J. Atmos. Sci.,* **63,** 2915–2930.

Franzke, C., S. Lee, and S. B. Feldstein, 2004: Is the North Atlantic Oscillation a breaking wave? *J. Atmos. Sci.,* **61,** 145–160.

Haynes, P. H., C. J. Marks, M. E. McIntyre, T. G. Shepherd, and K. P. Shine, 1991: On the downward control of extratropical diabatic circulations by eddy-induced mean zonal forces. *J. Atmos. Sci.,* **48,** 651–678.

Hurrell, J. W., 1995: Decadal trends in the North Atlantic Oscillation: Regional temperatures and precipitation. *Science,* **269,** 676–679.

——, Y. Kushnir, G. Ottersen, and M. Visbeck, 2003: *The North Atlantic Oscillation: Climate Significance and Environmental Impact*. *Geophys. Monogr.,* Vol. 134, Amer. Geophys. Union, 279 pp.

Kunz, T., K. Fraedrich, and F. Lunkeit, 2009a: Response of idealized baroclinic wave life cycles to stratospheric flow conditions. *J. Atmos. Sci.,* **66,** 2288–2302.

——, ——, and ——, 2009b: Synoptic scale wave breaking and its potential to drive NAO-like circulation dipoles: A simplified GCM approach. *Quart. J. Roy. Meteor. Soc.,* **135,** 1–19.

Kushner, P. J., and L. M. Polvani, 2004: Stratosphere–troposphere coupling in a relatively simple AGCM: The role of eddies. *J. Climate,* **17,** 629–639.

Lorenz, D. J., and D. L. Hartmann, 2003: Eddy–zonal flow feedback in the Northern Hemisphere winter. *J. Climate,* **16,** 1212–1227.

Martius, O., C. Schwierz, and H. C. Davies, 2007: Breaking waves at the tropopause in the wintertime northern hemisphere: Climatological analyses of the orientation and the theoretical LC1/2 classification. *J. Atmos. Sci.,* **64,** 2576–2592.

Matthewman, N. J., J. G. Esler, A. J. Charlton-Perez, and L. M. Polvani, 2009: A new look at stratospheric sudden warmings. Part III: Polar vortex evolution and vertical structure. *J. Climate,* **22,** 1566–1585.

McIntyre, M. E., and T. N. Palmer, 1985: A note on the general concept of wave breaking for Rossby and gravity waves. *Pure Appl. Geophys.,* **123,** 964–975.

Perlwitz, J., and H.-F. Graf, 2001: Troposphere–stratosphere dynamic coupling under strong and weak polar vortex conditions. *Geophys. Res. Lett.,* **28,** 271–274.

——, and N. Harnik, 2003: Observational evidence of a stratospheric influence on the troposphere by planetary wave reflection. *J. Climate,* **16,** 3011–3026.

Rivière, G., and I. Orlanski, 2007: Characteristics of the Atlantic storm-track activity and its relation with the North Atlantic Oscillation. *J. Atmos. Sci.,* **64,** 241–266.

Scaife, A. A., J. R. Knight, G. K. Vallis, and C. K. Folland, 2005: A stratospheric influence on the winter NAO and North Atlantic surface climate. *Geophys. Res. Lett.,* **32,** L18715, doi:10.1029/2005GL023226.

Strong, C., and G. Magnusdottir, 2008: Tropospheric Rossby wave breaking and the NAO/NAM. *J. Atmos. Sci.,* **65,** 2861–2876.

Thompson, D. W. J., and J. M. Wallace, 1998: The Arctic Oscillation signature in the wintertime geopotential height and temperature fields. *Geophys. Res. Lett.,* **25,** 1297–1300.

——, J. C. Furtado, and T. G. Shepherd, 2006: On the tropospheric response to anomalous stratospheric wave drag and radiative heating. *J. Atmos. Sci.,* **63,** 2616–2629.

Thorncroft, C. D., B. J. Hoskins, and M. E. McIntyre, 1993: Two paradigms of baroclinic-wave life-cycle behaviour. *Quart. J. Roy. Meteor. Soc.,* **119,** 17–55.

Vallis, G. K., E. P. Gerber, P. J. Kushner, and B. A. Cash, 2004: A mechanism and simple dynamical model of the North

Atlantic Oscillation and annular modes. *J. Atmos. Sci.,* **61,** 264–280.

Wallace, J. M., 2000: North Atlantic Oscillation/annular mode: Two paradigms—One phenomenon. *Quart. J. Roy. Meteor. Soc.,* **126,** 791–805.

Wittman, M. A. H., L. M. Polvani, R. K. Scott, and A. J. Charlton, 2004: Stratospheric influence on baroclinic lifecycles and its connection to the Arctic Oscillation. *Geophys. Res. Lett.,* **31,** L16113, doi:10.1029/2004GL020503.

——, A. J. Charlton, and L. M. Polvani, 2007: The effect of lower stratospheric shear on baroclinic instability. *J. Atmos. Sci.,* **64,** 479–496.

Woollings, T., B. Hoskins, M. Blackburn, and P. Berrisford, 2008: A new Rossby wave breaking interpretation of the North Atlantic Oscillation. *J. Atmos. Sci.,* **65,** 609–626.

Yu, J.-Y., and D. L. Hartmann, 1993: Zonal flow vacillation and eddy forcing in a simple GCM of the atmosphere. *J. Atmos. Sci.,* **50,** 3244–3259.